Graz University of Technology

Bachelor thesis

Institute of Theoretical and Computational Physics

Pressure-driven water translocation through short flexible carbon nanotubes

Thomas Brunner (12018550)

Supervisor: Ass.Prof. Douwe Jan Bonthuis

UF 033 678
SS23

11.06.2023

Contents

Abstract

The fluid dynamics of water in carbon nanotubes has been a subject of considerable interest in recent years due to advancements in measurement and manufacturing techniques for nanofluidic devices. Experimental studies have revealed intriguing flow characteristics of water in carbon nanotubes, including enhanced flow rates and slip length phenomena. These observations challenge the conventional assumptions of continuum theory used to describe fluid flow in macroscopic systems. In this thesis molecular dynamics (MD) simulations are used to investigate the behaviour of water in carbon nanotubes at the microscopic scale. These simulations provide valuable insights into the dynamics and interactions of water molecules within the confined nanotube environment. By creating a system which simulates a pressure-driven flow, a comparison to analytical solutions for pipe flows in the context of the Navier-Stokes equations is made. The finite element method is also employed to solve the Stokes equation of a model system with adapted boundary conditions. At last, the results found in this work are discussed and compared to the vast literature in the field.

1 Acknowledgements

First and foremost, I am most grateful to my parents. Their unconditional support, unwavering belief in me and continuous encouragement has been the driving force behind my accomplishments. Their presence have enabled me to pursue my dreams and reach my goals. I am forever indebted to them for their help when I needed it, their patience when I was demanding and their motivation to excel in being great parents.
I would also like to extend my appreciation to my sister, my girlfriend and my friends, who have been an endless source of moral support due to always having an open ear for my struggles.
I would like to express my sincere gratitude to my thesis advisor, Professor Douwe-Jan Bonthuis. His guidance and expertise have not only refined my work but also broadened my intellectual horizons. His lectures and especially the exercises of the university course Computational Physics have sparked the beginning of my interest in numerical methods and simulation. Through this curiosity, I was able to discover many fascinating research topics in the area of computational physics and their application to other sciences and technology.
I would also like to extend my appreciation to the faculty members and staff of Graz University of Technology and University Graz, whose expertise in and dedication to teaching have contributed to my overall academic development. Their passion for physics, its applications and willingness to share their knowledge through many interesting lectures have enriched my educational experience. Due to his impact on this thesis and my interests in general, I want to mention Professor Wolfgang von der Linden for his excellent lecture on continuum mechanics. The combination of fluid mechanics with my interests in numerical methods has led to this thesis and will surely continue to shape my academic journey.

2 Introduction

The efficient transport of water is essential for many processes, ranging from desalination and filtration to energy conversion. Over time, scientists and engineers have been researching various methods to optimize the efficiency of water transport in macroscopic systems. In recent years, the water transport properties of carbon nanotubes have gathered much attention in the field of nanofluidics, because of their observed enhanced flow rates at small scales. Possibilities for novel methods of efficient water desalination and filtration using these properties have been proposed.
The ability to control water at the molecular level within nanometer-scaled channels is also of great interest due to its occurrence in biological systems, such as ion channels in cell membranes. Carbon nanotubes offer a promising platform for studying the behaviour of water under nanoscale confinement due to their simple geometric structure. By exploiting the enhanced transport properties, it is thought to be possible to design innovative devices that can revolutionise technical processes. Understanding the fundamental principles governing these flows is therefore crucial for advancing the field, with the possibility of changing the world by increasing access to clean drinking water across water-poor countries.
The primary objective of this thesis is to introduce, investigate and analyse the mechanisms underlying water flow through carbon nanotubes. By exploring the fundamental principles governing the behaviour of water molecules in these systems, this thesis aims to introduce the author to the field of nanofluidics, replicate existing results and get insights into the potential applications of carbon nanotube based systems. The research objectives of this work are:

- Exploring the research field through hands-on simulation and data analysis work
- Investigating the influence of the carbon nanotubes diameter
- Analysing the effects of varying the pressure gradient on the water transport
- Studying the role of tube flexibility by changing bond parameters
- Trying to adapt continuum models to better capture microscopic effects

In chapter 3 the fundamentals of fluid mechanics, such as the Navier-Stokes equations, the Reynolds number and the Hagen-Poiseuille equation will be explained. Molecular effects of water in the microscopic scale will be shown to see the differences in contrast to continuum mechanics. Chapter 4 will give an overview to the methodology used in this thesis. This includes the molecular dynamics setups, simulation parameters and the application of mixed finite element methods to the Stokes equation. A table of the carried-out molecular dynamics simulations, which led to the results shown in this work, is given in Chapter 5. In chapter 6 the analysis of the simulations is conducted by showing velocity profiles, calculating slip lengths, checking the volume fluxed against the classical laws, showing the effects of varying the parameters and showing a model simulated with the finite element method. To compare to the literature we discuss the obtained results in chapter 7. Chapter 8 concludes this thesis by giving an outlook on the research field.

3 Theory

3.1 Continuum theory

The overarching research question in this work is on the validity of continuum theory on nanoscales and on how one can adjust known fluid dynamics laws like the Hagen-Poiseuille equation to better describe flows at this length scale. Therefore in chapter 3.1.1 we shall first explain the basics of fluid mechanics. We then explain macroscopic pipe flow and microscopic adjustments to better describe effects like velocity slippage. We of course, also have to consider molecular effects like the polarity of water or hydrophobicity, which will be done to sum up the further needed theoretical knowledge.

3.1.1 Navier-Stokes equations

The governing equations of fluid dynamics are the Navier-Stokes equations. A derivation of these equations can be found in any book about continuum or fluid mechanics [1]. The general form of the Navier-Stokes equations which can be derived from the Cauchy momentum equation is

$$\rho\frac{D\mathbf{u}}{Dt} = \rho(\frac{\partial\mathbf{u}}{\partial t} + (\mathbf{u}\nabla)\mathbf{u}) = -\nabla p + \nabla\cdot\boldsymbol{\tau} + \mathbf{f} \tag{1}$$

With the deviatoric part of the Cauchy stress tensor $\boldsymbol{\tau}$ and the pressure p which describes the normal stress in the fluid. Calculating the divergence of the deviatoric stress tensor $\boldsymbol{\tau}$ by using the Stokes stress constitutive equation and plugging in the strain-rate tensor $\boldsymbol{\varepsilon}$ one gets

$$\boldsymbol{\tau} = 2\eta\boldsymbol{\varepsilon} = \eta(\nabla\mathbf{u} + \nabla\mathbf{u}^T) \tag{2}$$

Using some tensor identities ($\nabla\cdot(\nabla\mathbf{u}) = \Delta\mathbf{u}$ and $\nabla\cdot(\nabla\mathbf{u})^T = \nabla(\nabla\cdot\mathbf{u})$) and then using the incompressibility condition $\nabla\cdot\mathbf{u} = 0$ the divergence of the deviatoric stress tensor results as

$$\nabla\cdot\boldsymbol{\tau} = \eta\Delta\mathbf{u} \tag{3}$$

Plugging this in the general form of the Navier-Stokes equation the incompressible equations follow

$$\rho\frac{D\mathbf{u}}{Dt} = \rho(\frac{\partial\mathbf{u}}{\partial t} + (\mathbf{u}\nabla)\mathbf{u}) = -\nabla p + \eta\Delta\mathbf{u} + \mathbf{f} \tag{4}$$

3.1.2 Reynolds number, the laminar regime and Stokes flow

By comparing the magnitude of the terms of the incompressible equation with the help of similarity theory [1] and dimensional analysis, the scaling of the convective term (which is responsible for turbulent phenomena in fluids)

$$(\mathbf{u}\nabla)\mathbf{u} \simeq \mathcal{O}(\frac{U^2}{L}) \tag{5}$$

and the viscous term (which opposes the turbulent behaviour of the convective term)

$$\eta \Delta \mathbf{u} \simeq \mathcal{O}(\frac{\nu U}{L^2}) \tag{6}$$

can be estimated. The ratio of both terms is a statement about the turbulence of a system. This can be done using a characteristic velocity scale U, a characteristic length scale L and the kinematic viscosity ν of the fluid.

$$\frac{(\mathbf{u}\nabla)\mathbf{u}}{\nu \Delta \mathbf{u}} \simeq \mathcal{O}(\frac{UL}{\nu}) = \mathcal{O}(Re) \tag{7}$$

The resulting characteristic dimensionless quantity is called the Reynolds number Re

$$Re = \frac{UL}{\nu} = \frac{\rho UL}{\eta} \tag{8}$$

The turbulent behaviour of a system also depends on the type of system (e.g. pipe flow, open flow). Thus for different systems, a critical Reynolds number Re_{crit} can be experimentally determined. In the case of Hagen-Poiseuille pipe flow the critical Reynolds number in the literature [1] is

$$Re_{crit} \approx 2300 - 2500 \tag{9}$$

Assuming that the Reynolds number Re of a system is small compared to the critical Reynolds number Re_{crit} one can assume laminar flow and therefore leave out the negligible convective term. The resulting equation is called the Stokes equation. The stationary form of the Stokes equation together with the incompressibility condition is

$$\eta \Delta \mathbf{u} - \nabla p + \mathbf{f} = 0 \text{ in } \Omega \tag{10}$$

$$\nabla \cdot \mathbf{u} = 0 \text{ in } \Omega \tag{11}$$

To formulate a boundary value problem one also employs Dirichlet boundary conditions of the form

$$\mathbf{u} = \mathbf{u}_D \text{ in } \partial\Omega \tag{12}$$

$$\tag{13}$$

3.1.3 Slip length & Hagen–Poiseuille equation

In fluid mechanics the pressure-driven flow through a cylinder with diameter d and length L is described by a parabolic profile which is called pipe or Hagen-Poiseuille flow. In the macroscopic case the flow velocity at the wall is set to be zero, which is called a no-slip condition.

$$\mathbf{u}|_{r=\frac{d}{2}} = \mathbf{0} \tag{14}$$

Given the geometry cylindrical coordinates are used. Through a symmetry argument one can easily see that the velocity $\mathbf{u}$ may not depend on the coordinate z along the flow axis (translational invariance) and should be axisymmetric along the flow axis. The derivation of the solution of the Stokes equation in this geometry can be found in the book [1]. The resulting velocity distribution inside of the cylinder follows as

$$u_z(r) = \frac{\Delta p}{16\eta L}(d^2 - 4r^2) \tag{15}$$

Through integrating the velocity profile over the cross section one gets a relation between the pressure difference Δp and the volumetric flow rate Q. The relation is called Hagen–Poiseuille law and is given by

$$\Delta p = \frac{128\eta Q L}{\pi d^4} \tag{16}$$

In the microscopic case of flows on the nanometer scale it seems that the macroscopic no-slip condition can no longer be employed [2]. The reason for this will be further illustrated in the next subsection 3.3. Instead a slip condition is employed using a characteristic parameter which is called the slip length b [2]. The corresponding slip boundary condition

$$-b\frac{\partial}{\partial r}u_z|_{r=\frac{d}{2}} = u_z|_{r=\frac{d}{2}} \tag{17}$$

describes the distance at which the linear continuation of the flow profile reaches zero. This condition can be understood more easily through the following figure 1.

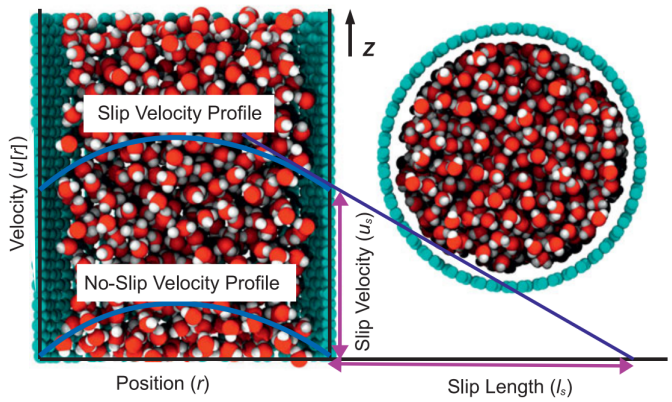

Figure 1: Illustration of the slip length b reproduced from [3]

If one employs such a boundary condition on the axisymmetric pipe flow problem [4], the resulting velocity distribution

$$u_z(r) = -\frac{\Delta p}{16\eta L}(d^2 + 4bd - 4r^2) \tag{18}$$

follows. The corresponding modified Hagen-Poiseulle law can be found by substituting

$$Q_{slip} = Q_{classical}(1 + \frac{8b}{d}) \tag{19}$$

into the original equation [5].

3.2 Entrance resistance

In both macro- and microscopic flows the transition from bulk to pipe flow has an entrance resistance. This resistance causes a pressure difference which needs to be overcome by the fluid to flow into the pipe. In the case of Stokes flow the pressure drop can be modelled by the following equation obtained from [6], where R is the radius of the aperture.

$$\Delta p = 3\frac{3\eta}{R^3}Q \tag{20}$$

3.3 Molecular behaviour of water

The behaviour of water at interfaces on the microscopic scale depends mainly on the chemical nature of the interface material. Substances are classed by their relationship with water into hydrophilics and hydrophobics. Hydrophilic materials are attracted to water which results in larger friction and smaller flow rates. Often hydrophilic molecules have polar OH groups which interact with the polarity of water. Hydrophilic interfaces are prominent in biological systems, for example in membrane proteins such as ion channels [7]. Hydrophobic materials are thus classified as those substances which are not attracted to water. Therefore they are usually not or only weakly polar.
Examples for small hydrophobic systems are the here describe carbon nanotubes. It is obvious that these two different types of water attraction must influence the flow field.
In macroscopic fluid mechanics, a solid wall is most commonly modelled by a no-slip condition. This means that both the normal as well as the tangential velocity components vanish at a wall. The normal component must be zero because of the impermeability through and the absolute rigidity of the wall. The argument why the tangential component must disappear, however is, not obvious at all. Historically the no-slip condition was first observed experimentally and accepted without a theoretical explanation. The first discrepancies which showed differences to a no-slip condition where found in rarefied gas flows. Here it is not obvious at all why matter should stick to the wall. Maxwell worked on flow slippage on interfaces during his works on kinetic gas theory [8]. Because of this the classic slip boundary condition is also named Maxwell-slip condition. In rarefied gases the Knudsen number also plays an important role due to describing the relationship between free path length and the geometrical size of a system. [9][10]. This shall however not be described in more detail in this work due to a focus on liquid flows, where the free path length is of the order of the molecular radius. Simulations and experiments using water flows in carbon nanotubes indicate large slip lengths [3]. It has to be noted, however, that results differ quite substantially depending on simulation parameters, the helicity of the nanotube or used water models.

To explain slip in microscopic systems another approach is also common. It uses a radially-dependent viscosity which can explain higher velocities at the interface [5]. It is also thought that the hydrophobic nature of carbon may result in small gas gaps or depletion layers due to hydrogen-bonds overwhelming the water-carbon interactions.

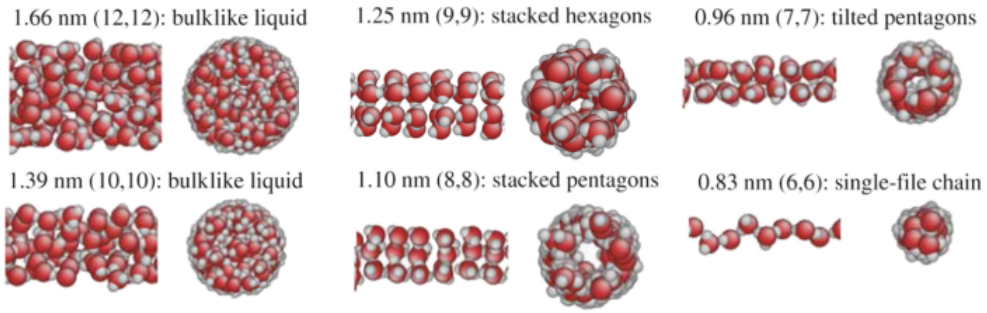

Figure 2: Structuring: Arrangements of water molecules in different diameter sized nanotubes due to the confinement and hydrogen bonds. This image was reproduced from [11]

The question of to what extent continuum mechanical models hold in nanometer sized systems is also heavily discussed. According to [2] the bulk Navier-Stokes equations hold up to confinements of a few nanometers. The authors of [12] review existing work on this topic and list many different previously found length scales. They also find that after around 150 molecular diameters no deviation to the macroscopic laws is expected, independent of surface force effects. To sum up, it is very difficult to find generally applicable consistent rules regarding nanoflows described by continuum theory. One also has to address the effect of water polarity. Due to the hydrogen bonds the water molecules arrange themselves energetically optimal. In bulk water, these arrangements change very fast in time due to internal fluctuations. In nanometer sized channels, which only have a diameter of a few molecular radii, the waters arrange themselves and then keep this arrangement until the molecules are in bulk again due to the confinement. This effect is called structuring and is displayed in Figure 2 for multiple carbon nanotube sizes. This effect also describes the density profiles of water in small nanotubes. In these nanotubes, the molecules arrange themselves in layers. Whereby in each layer there are multiple waters. If the size of the nanotube is just right the density is zero in the middle. Examples of density profiles in different size carbon nanotubes are shown in the following figure 3. Much of these density distributions can already be explained by close-sphere packing in cylinders, which show similar profiles.

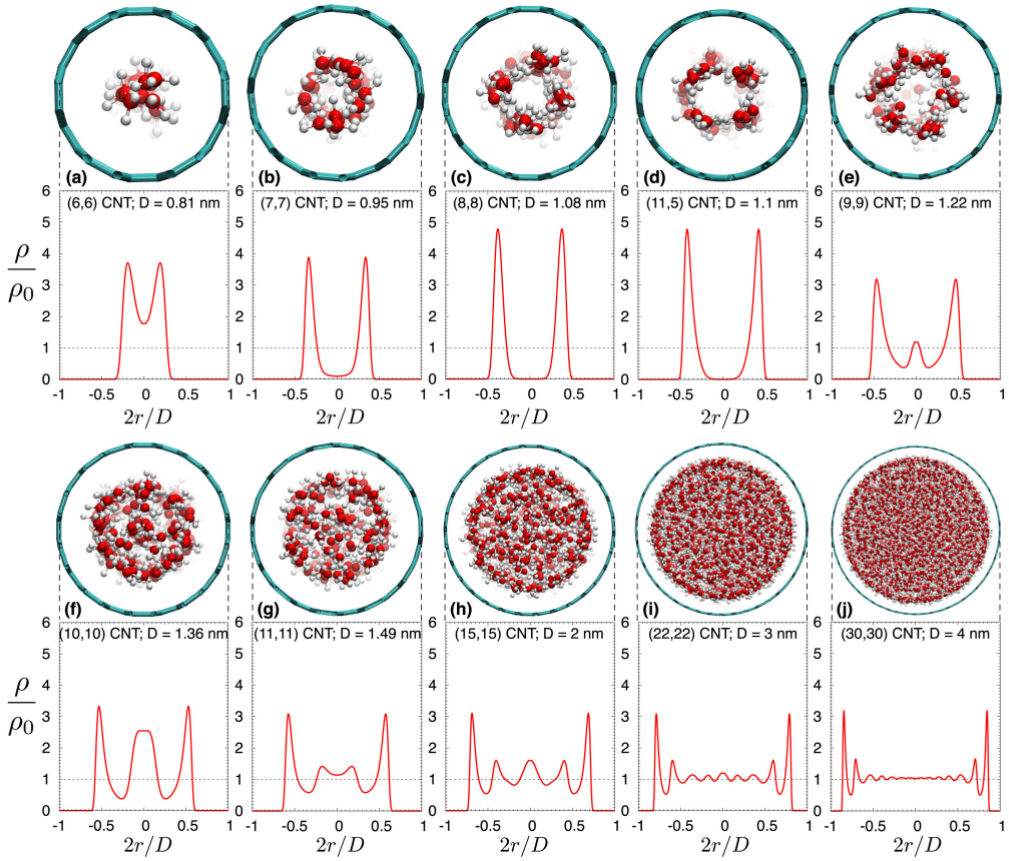

Figure 3: Density profiles of water molecules in small carbon nanotubes. This image was reproduced from [13]

4 Methodology

4.1 Molecular dynamics

The molecular dynamics simulations were implemented and carried out using the open-source program GROMACS [14].

4.1.1 Simulation setup

To simulate the pressure-driven flow through a carbon nanotube a geometry was chosen which consists of two water reservoirs which are separated by two graphene sheets. These two sheets were fixated in space using a very stiff (k_b = 100000 kJmol^{-1}A^{-2}) harmonic potential.
Between the sheets, the carbon nanotube was added. At both entries of the nanotube the carbon atoms of the sheets were removed. To generate the pressure which induces the flow, another graphene sheet was added. The movement of this sheet is implemented by a *pull-code*. This algorithm applies a constant force on the atoms of the sheet.
The setup of the geometry was created using a self-written Python script. The geometry of graphene and the used nanotubes were imported by the script using the *.xmol*-file format. This script carried out the positioning of the sheets and the tube. The geometry of the cell was then adjusted to create infinite layers of graphene to match the periodic boundary conditions. The solvation of the system with randomly oriented SPC/E-water molecules was implemented.

Table 1: SPC/E water model parameters [15] [16]

parameter	value	unit
σ	3,166	Å
ϵ	0,65	kJ/mol
r_{OH}	1	Å
θ_{HOH}	109,47	°
q_O	-0,847	e
q_H	-q_O/2	e

The bonds of the graphene sheets and the nanotube were calculated and could be individually assigned different spring constants. At the end the geometry was written out in a *.gro*-file and the information about the atoms (Lennard-Jones parameters, mass, bonds) was written out in *.itp*-files.

Table 2: Carbon parameters

parameter	value	unit
σ	3,581	Å
ϵ	0,2775	kJ/mol
r_{CC}	1,421	Å
θ_{CCC}	120	°
q_C	0	e

The following three geometries were created for the simulations

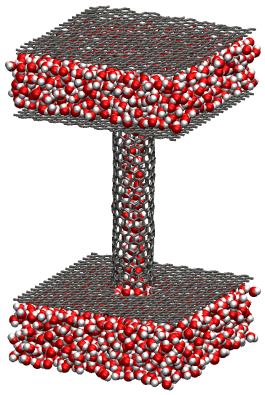

Figure 4: Geometry with a (13, 0)-nanotube

parameter	value
(n, m)	(13, 0)
d_{CNT}	1,02 nm
l_{CNT}	5,00 nm
n_{WAT}	2420
n_{CAR}	2188
$h_{Reservoir}$	4,61 nm
$w_{Reservoir}$	4,55 nm
$l_{Reservoir}$	1,50 nm

Table 3: Geometry parameters

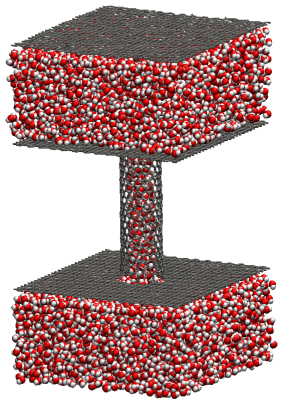

Figure 5: Geometry with a (18, 0)-nanotube

parameter	value
(n, m)	(18, 0)
d_{CNT}	1,41 nm
l_{CNT}	5,00 nm
n_{WAT}	9736
n_{CAR}	4036
$h_{Reservoir}$	6,76 nm
$w_{Reservoir}$	6,32 nm
$l_{Reservoir}$	3,00 nm

Table 4: Geometry parameters

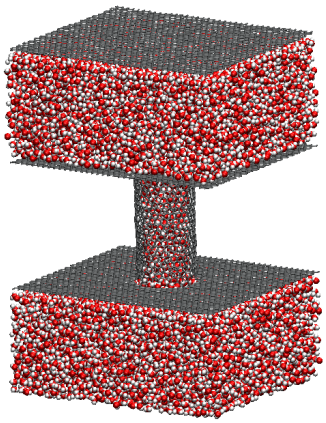

Figure 6: Geometry with a (30, 0)-nanotube

parameter	value
(n, m)	(30, 0)
d_{CNT}	2,35 nm
l_{CNT}	5,00 nm
n_{WAT}	21230
n_{CAR}	6620
$h_{Reservoir}$	8,98 nm
$w_{Reservoir}$	8,02 nm
$l_{Reservoir}$	4,00 nm

Table 5: Geometry parameters

4.1.2 Simulation steps

The common workflow to equilibrate a system in MD-simulations is a combination of an energy-minimization step, a NVT-step and a NPT step. This is then followed by the main step, which is commonly referred to as the "production" run. In the first step, the potential energy gets minimized by shifting and rotating all (specified) atoms of the system. An example plot of a energy-minimization can be seen in Figure 27. In this work, the minimization is carried out using a steepest-descent algorithm.

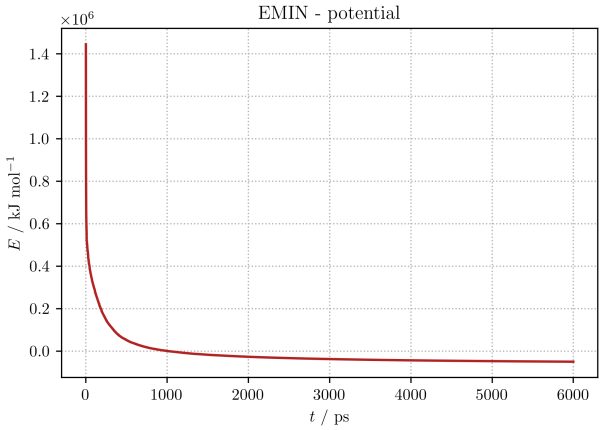

Figure 7: Potential convergence in energy minimization.

In the NVT-step a canonical-ensemble is simulated by conserving the particle number N, the volume V of the system and the temperature T. To control the total energy of the system and hold the temperature T constant, a thermostat algorithm is used. This algorithm tries to approximate the canonical ensemble by adding/removing energy to/from the system. In this work, a *V-rescale* thermostat which scales the volume V of the system, was used. In the following Figure 8 the temperature of a simulated system in the NVT-step can be seen. The behaviour of the pressure in the same simulation is also shown.

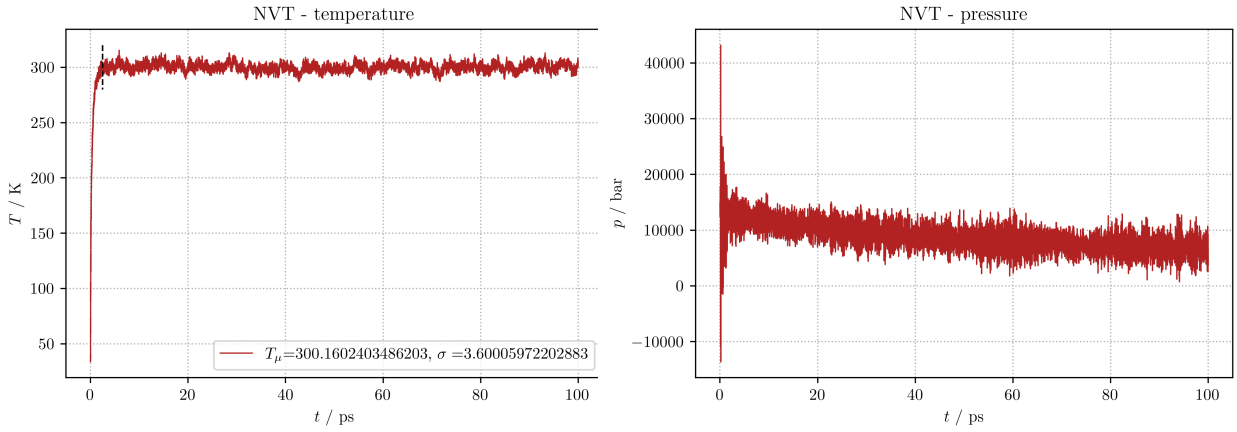

Figure 8: Temperature and pressure in NVT.

In the NPT-step a barostat is added to the thermostat. These two algorithms try to approximate an isothermal–isobaric ensemble by conserving the particle number N, the

pressure P and the temperature T. Here, a *Berendsen* algorithm [17] is used which scales the velocities of the particles. The trajectories of the temperature T and pressure p during a NPT-step are visualized in the following figure 9.

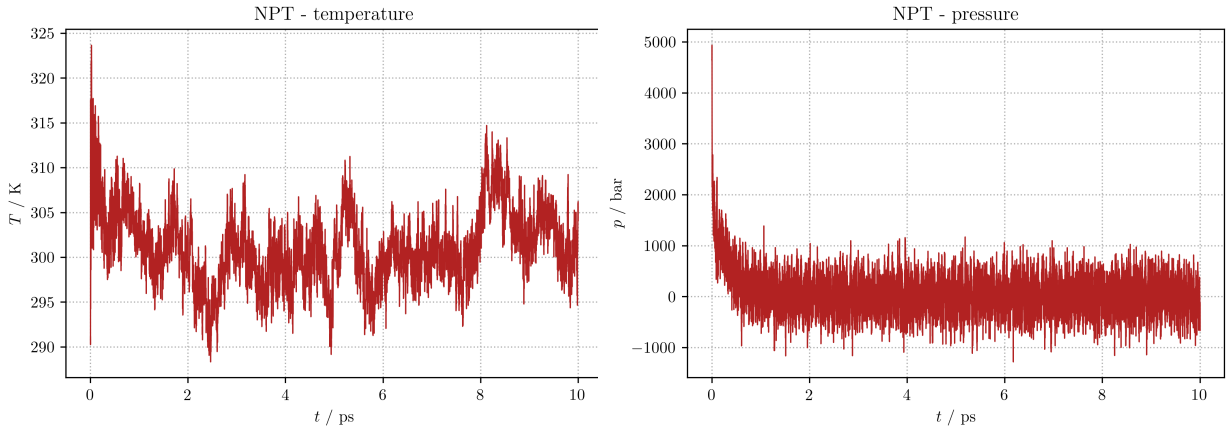

Figure 9: Temperature and pressure convergence in NPT.

After the NPT equilibriation, the main simulation of the system is carried out in a canonical-ensemble. The constant force pulling of the third graphene sheet is activated at the beginning of this step.

4.2 Finite element method

The finite element part of this work was carried out using the open-source package **FEnics** [18], which gives Python interfaces to C++ implementations of mesh generation, abstract definition of mathematical problems and efficient solvers for linear and nonlinear systems of equations.

4.2.1 Stokes flow - weak form

Since in the case of the Stokes equation, one has to approximate two different physical quantities (the pressure field p and the velocity field $\mathbf{u}$) one uses a mixed-finite element formulation [19]. The following definition of the mixed-finite element formulation is found in the literature[20]. The used function spaces for the Stokes system [20] are

$$V_g = \{v \in [H^1(\Omega)]^d : v|_{\partial\Omega} = g_D\} \tag{21}$$

$$Q = \{q \in L^2(\Omega) : (q, 1) = 0\} \tag{22}$$

Where V_g is the velocity space, $[H^1(\Omega)]^d = [W_k^2(\Omega)]^d$ is a Sobolev space of dimension d (for the definition of Sobolev spaces see e.g. [19][20]), Q is the pressure space and $(q, 1) = 0$, meaning that the pressure has zero mean value on the domain. This is to set an absolute reference point for the pressure field.
To obtain the weak form of the Stokes equation, one multiplies by a test vector $v \in V_0$ for the first equation and $q \in Q$ for the incompressibility equation. For all further steps to obtain the weak-form the reader is referenced to [20].
The resulting bilinear form $a(\cdot, \cdot)$ and linear form $f(\cdot)$ are

$$a((\mathbf{u}, p), (\mathbf{v}, q)) = L((\mathbf{v}, q)) \tag{23}$$

$$a((\mathbf{u}, p), (\mathbf{v}, q)) = \int_\Omega \nabla \mathbf{u} \cdot \nabla \mathbf{v} + \nabla \cdot (\mathbf{u}q - \mathbf{v}p) d\mathbf{x} \tag{24}$$

$$L((v, q)) = \int_\Omega \mathbf{v} \cdot \mathbf{f} d\mathbf{x} + \int_{\partial\Omega_N} \mathbf{g} \cdot \mathbf{v} ds \tag{25}$$

Different implementations with weakly imposed pressure boundary conditions and weakly imposed slip boundary conditions [21] were carried out but did not produce working results. This is why they are not described in detail in this work. There are many different ways to implement weak boundary conditions into finite element discretisations. The most popular versions use Lagrange multipliers, penalty formulations and the Nitsche method.

4.2.2 Finite element approximation with Taylor-Hood elements

The finite element approximation of the weak form can be formulated using functions $u_h \in V_h$ and $p_h \in P_h$ in finite dimensional subspaces. Using the Galerkin method which uses the same function spaces for approximating the test functions v one gets

$$a(u_h, v) + b(v, p_h) = l(v) \quad \forall v \in V_h \tag{26}$$

$$b(u_h, q) = 0 \quad \forall q \in P_h \tag{27}$$

The functions u_h and p_h can then be expressed using a basis functions φ_i and χ_i as

$$u_h = \sum_i \xi_i \varphi_i, \quad p_h = \sum_i \psi_i \chi_i \tag{28}$$

The linear system of equations can then be written as

$$\begin{bmatrix} a(\varphi_j, \varphi_i) & b(\varphi_i, \chi_j) \\ b(\varphi_j, \chi_i) & 0 \end{bmatrix} \begin{bmatrix} \xi \\ \psi \end{bmatrix} = \begin{bmatrix} b \\ 0 \end{bmatrix} \tag{29}$$

This is a so-called saddle point problem, which is known to be hard to solve. In the Stokes system, the function spaces V_h and P_h for the approximation have to chosen wisely to meet the so-called *Discrete Inf-Sup-* or *LBB-* condition which guarantees a unique solution [19]. The most common choice in incompressible fluid mechanics is to use continuous piecewise quadratic functions for each velocity component and continuous piecewise linear functions for the pressure field. These widely used finite elements are called *Taylor-Hood* elements [20].

5 Results

5.1 MD simulation data

Table 6: Carried out molecular dynamics simulations.

System	Nr.	t / ps	F / kJ mol^{-1}nm^{-1}	k_b / kJ/(mol nm^2)
(13, 0)	0	100	$1,0 \cdot 10^5$	$1,0 \cdot 10^4$
	1	100	$1,0 \cdot 10^5$	$2,5 \cdot 10^4$
	2	100	$1,0 \cdot 10^5$	$5,0 \cdot 10^4$
	3	100	$1,0 \cdot 10^5$	$7,5 \cdot 10^4$
	4	100	$1,0 \cdot 10^5$	$1,0 \cdot 10^5$
	5	100	$1,0 \cdot 10^5$	$2,5 \cdot 10^5$
	6	100	$1,0 \cdot 10^5$	$5,0 \cdot 10^5$
	7	100	$1,0 \cdot 10^5$	$7,5 \cdot 10^5$
	8	100	$1,0 \cdot 10^6$	$1,0 \cdot 10^6$
	9	100	$1,0 \cdot 10^6$	$2,0 \cdot 10^6$
	10	100	$1,0 \cdot 10^3$	$3,2 \cdot 10^6$
	11	100	$5,0 \cdot 10^3$	$3,2 \cdot 10^6$
	12	100	$1,0 \cdot 10^4$	$3,2 \cdot 10^6$
	13	100	$5,0 \cdot 10^4$	$3,2 \cdot 10^6$
	14	100	$1,0 \cdot 10^5$	$3,2 \cdot 10^6$
	15	100	$2,0 \cdot 10^5$	$3,2 \cdot 10^6$
	16	100	$3,0 \cdot 10^5$	$3,2 \cdot 10^6$
	17	100	$4,0 \cdot 10^5$	$3,2 \cdot 10^6$
	18	100	$5,0 \cdot 10^5$	$3,2 \cdot 10^6$
	19	100	$1,0 \cdot 10^6$	$3,2 \cdot 10^6$
	20	100	$1,0 \cdot 10^6$	$4,1 \cdot 10^6$
	21	100	$1,0 \cdot 10^6$	$5,0 \cdot 10^6$
(18, 0)	22	100	$5,0 \cdot 10^4$	$3,2 \cdot 10^6$
(30, 0)	23	100	$7,5 \cdot 10^4$	$3,2 \cdot 10^6$
	24	100	$1,0 \cdot 10^5$	$3,2 \cdot 10^6$
	25	100	$1,8 \cdot 10^5$	$3,2 \cdot 10^6$
	26	100	$2,5 \cdot 10^5$	$3,2 \cdot 10^6$
	27	100	$4,0 \cdot 10^5$	$3,2 \cdot 10^6$
	28	100	$5,0 \cdot 10^5$	$3,2 \cdot 10^6$

5.2 Molecular dynamics

The output data of the different simulations (which were listed in chapter 5.1) consisted of trajectory files and information about the different physical quantities, which varied during time steps.
To save on disk space the trajectory data of all atoms was only saved every 1000 steps. This reduces the temporal correlations which are apparent when one thinks about the occurrence of structuring as discussed earlier 2. To give an overview on the fluid flow in the three systems, we start by showing the flow patterns.

5.2.1 Density profiles

To visualize this structured flow pattern, as an example a single time step of a simulation is shown in Figure 10. It can be seen that the water molecules are arranged in packs of four in each layer. This matches with the earlier presented Figures 2 & 3, which showed structuring and the density profiles inside nanotubes.

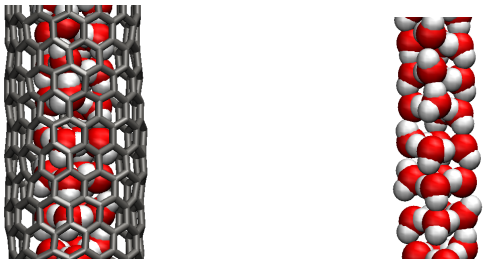

Figure 10: A sample timestep from a molecular dynamics simulation of the (13,0) nanotube to show the effect of structuring in small nanotubes.

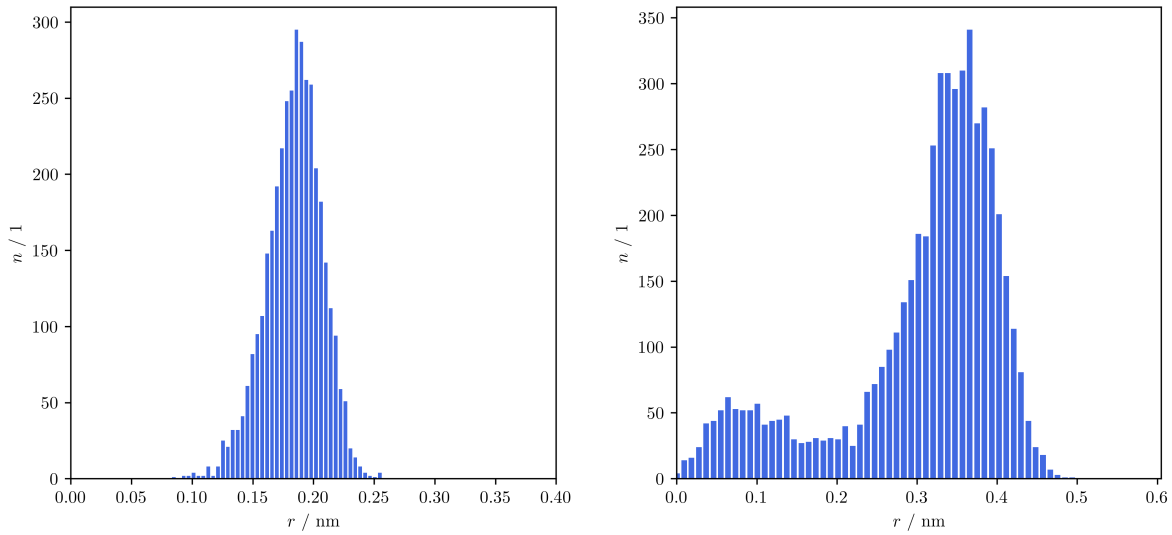

Figure 11: An example of the density profiles $n(r)$ of the water molecules in the (13,0) and (18,0) nanotube.

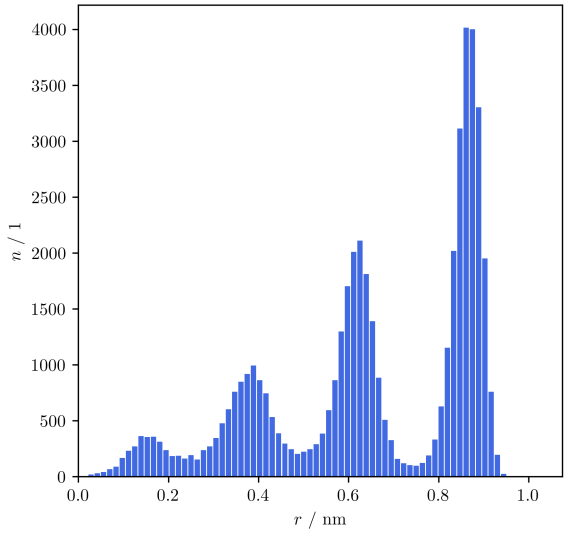

Figure 12: An example of the density profiles $n(r)$ of the water molecules in the (30,0) nanotube.

5.2.2 Velocity profiles

In the smallest nanotube the structuring effect of the molecules can be seen easily by plotting the axial velocity component u_z as a function of the radius r. To mitigate the effect of entrance and exit effects, only the waters in the central part (3 out 5 nm) of the nanotube were considered. The data points were binned by velocity and radial position. As the amount of particles in each bin depends on the simulation time, the linear colour scale should only show a qualitative distribution. In the following Figures 13 & 14 the pull force F was varied to see the effect of higher pressures on the flow. The water molecules are arranged in a way that no single molecule is ever found near the centre of the nanotube.

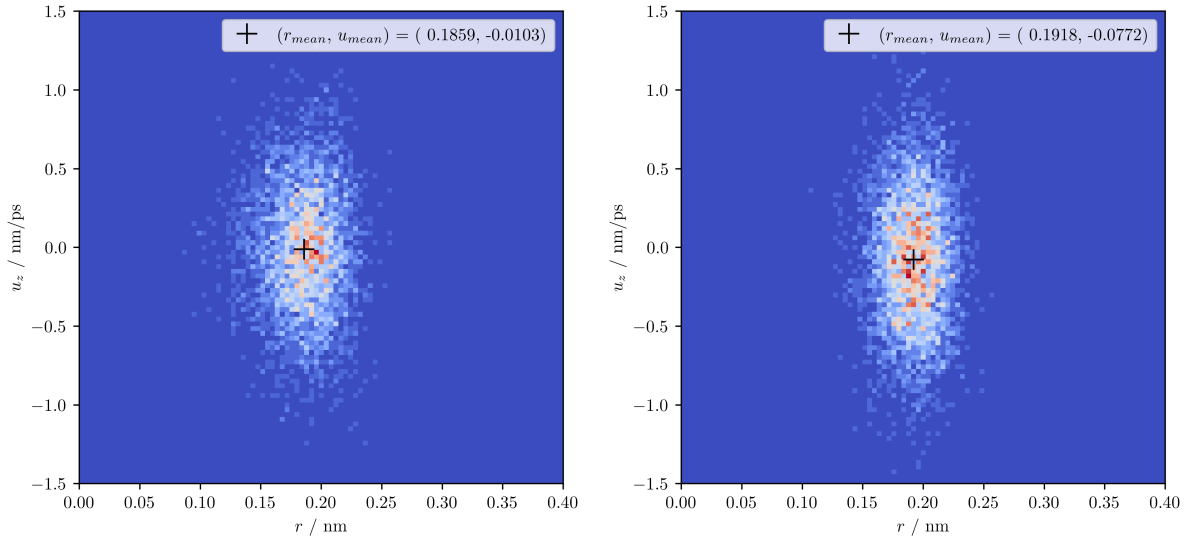

Figure 13: The velocity profiles $u_z(r)$ in the (13,0) nanotube. On the left the pull force $F = 10000\text{kJ mol}^{-1}\text{nm}^{-1}$ and on the right $F = 50000\text{kJ mol}^{-1}\text{nm}^{-1}$

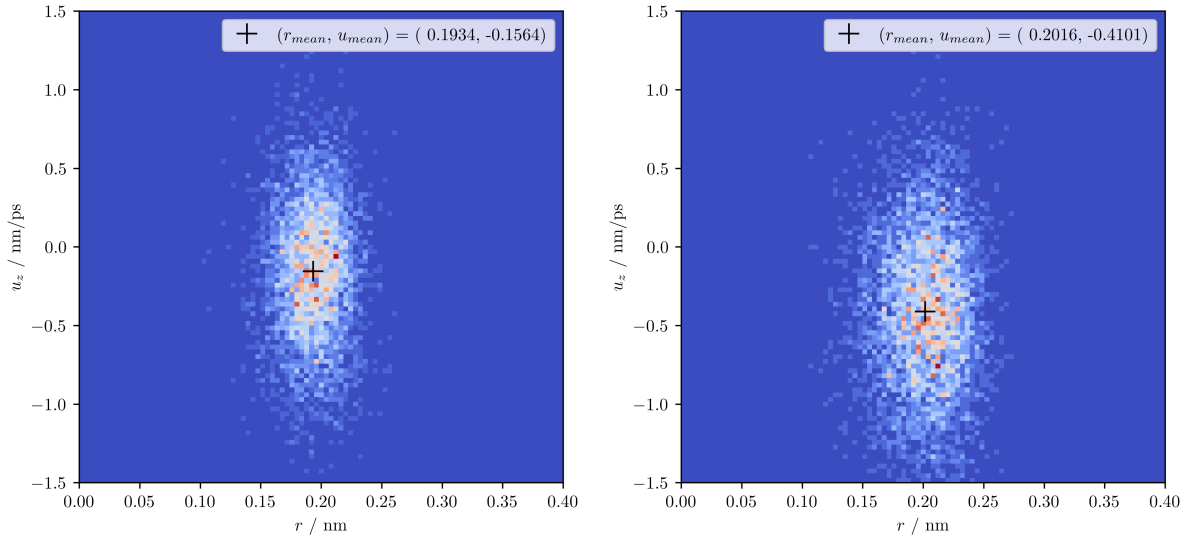

Figure 14: The velocity profiles $u_z(r)$ in the (13,0) nanotube. On the left the pull force $F = 100000\text{kJ mol}^{-1}\text{nm}^{-1}$ and on the right $F = 250000\text{kJ mol}^{-1}\text{nm}^{-1}$

An attempt was made to recover a parabolic flow profile or the slip length b through this data. But this was not possible in this nanotube. In the search of a parabolic profile the next larger (18,0) nanotube was examined. In Figure 19, the results can be seen. In this system the data showed no underlying hint on a classical pipe flow profile. Thus, also the determination of the slip length b is impossible.

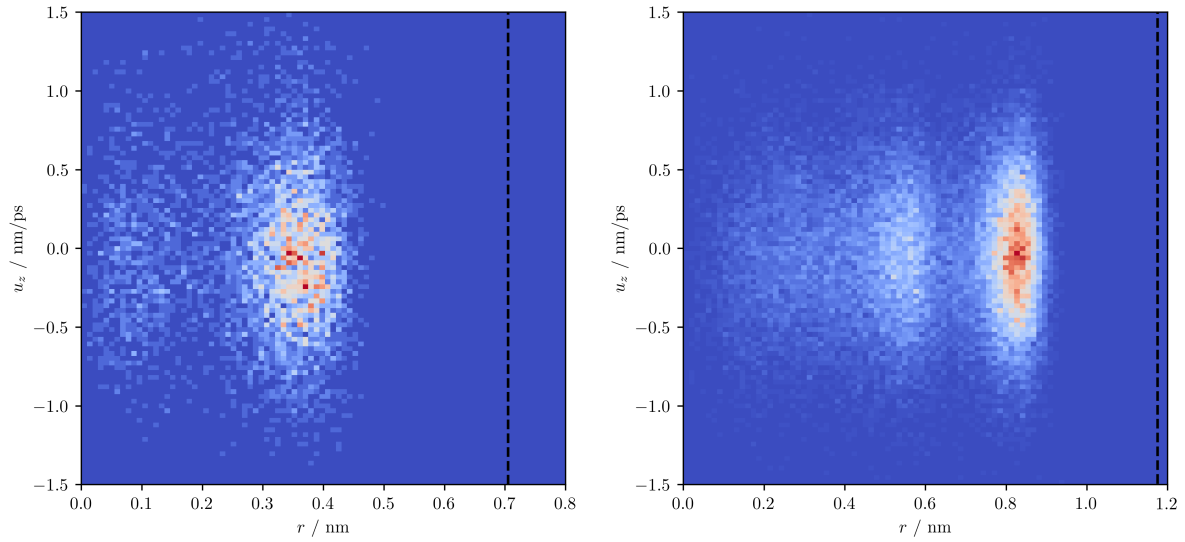

Figure 15: The velocity profiles $u_z(r)$ in the (18,0) nanotube (left) and the (30,0) nanotube (right). The pull force is $F = 100000\text{kJ mol}^{-1}\text{nm}^{-1}$.

5.2.3 Slip length through regression

Out of the simulations of the (30,0) systems parabolic flow profile (for example as shown in following Figure 16) could be extracted.

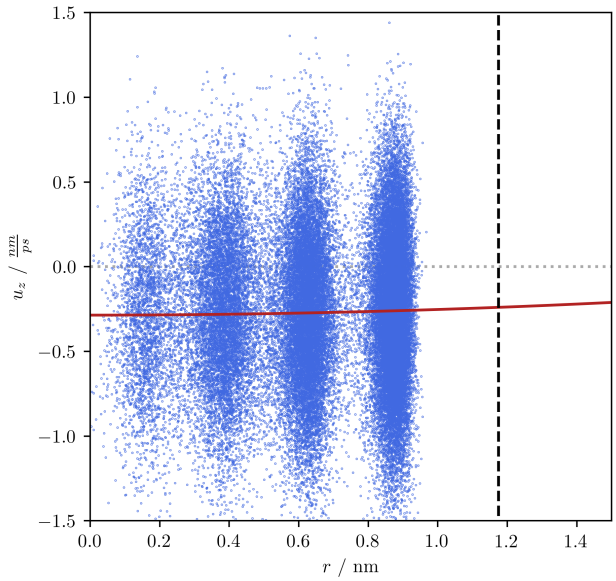

Figure 16: Data of the axial velocity u_z as a function of the radius r. In this case a pull force of $F = 500000$ kJ/(mol nm) was used. The red line is the fitted parabolic profile. The slip length b was extracted by differentiating the fit at the carbon nanotube radius and linearly extending of the flow domain.

This was carried out for a range of different pull forces F. The slip velocity u_{slip} and the slip length b are shown as a function of the applied pull force in the following Figure 17.

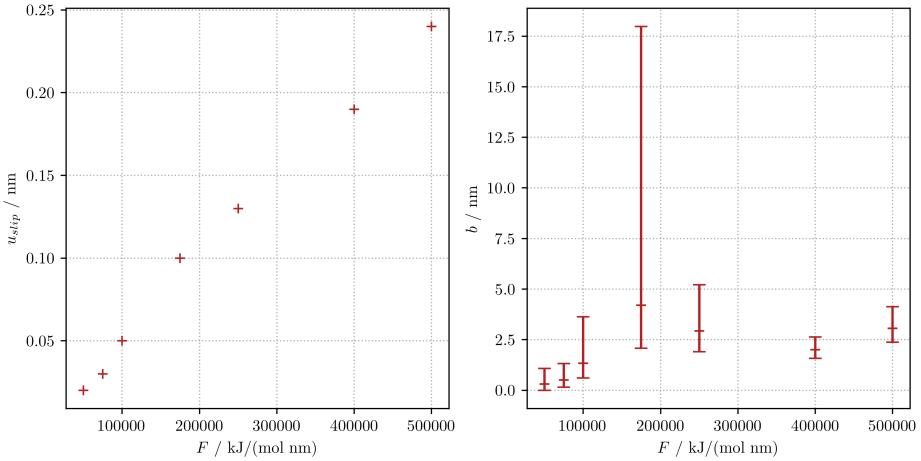

Figure 17: The slip velocity u_{slip} and the slip length b as a function of the pull force F. This was extracted from parabolic fits to $u_z(r)$ in the (30,0)-CNT system.

5.2.4 Microscopic Hagen-Poiseuille relation

To investigate the validity of the macroscopic linear relationship between pressure and velocity, the mean velocity $\langle u_z \rangle$ was extracted from the data of all simulations by averaraging over the CNT length and all time steps. The relationship is shown in Figure 18. A regression of all but the last few data points show the linearity of the underlying relationship over multiple orders of magnitude.

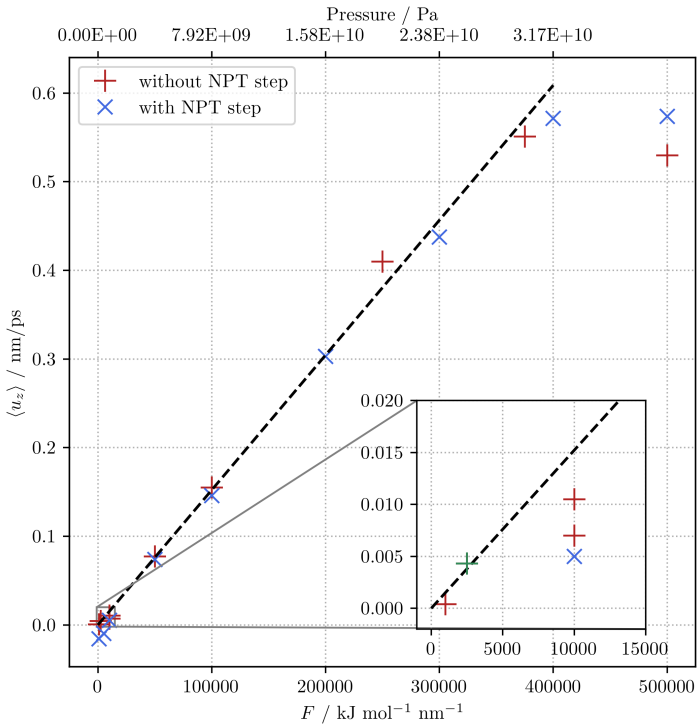

Figure 18: The mean axial velocity $\langle u_z \rangle$ as a function of the applied pull force F. Since the corresponding simulations were carried out with and without a NPT step, both are marked.

Out of the linear regression and the geometry of the system the following slip length b for the "microscopic" Hagen-Poiseuille equation 19 can be extracted.

$$\langle u_z \rangle = kF = 1.522 \cdot 10^{-6} F \tag{30}$$

By assuming a constant velocity across the radius and thus multiplying this equation with the cross-sectional area of the nanotube

$$Q_{slip} = \langle u_z \rangle R_{CNT}^2 \pi = kFR^2\pi \tag{31}$$

one can get a expression for the volume flux Q_{slip}. Then using the modified Hagen-Poiseuille law

$$Q_{slip} = Q_{classical}(1 + \frac{4b}{R}) = \frac{\Delta p R^4 \pi}{8\eta l_{CNT}}(1 + \frac{4b}{R}) \tag{32}$$

Using the two equations defined above, $\Delta p = F/A$, $\eta = 1$ mPa s and the values of the geometry A_{pull}, l_{CNT} and R one can arrive at

$$b = (\frac{8k\eta A_{pull} l_{CNT}}{R^2} - 1) \cdot \frac{R}{4} = 0,25 \text{ nm} \tag{33}$$

5.3 Volume flux

With the pull force F and the area of the puller sheet A_{pull} the classical continuum volume flux $Q_{continuum}$ can be calculated through the Hagen-Poiseuille equation as

$$Q_{continuum} = \frac{\pi r^4}{8\eta L} \frac{F}{A_{pull}} \tag{34}$$

Out of the molecular dynamics simulation data, the particle flux n through the carbon nanotubes were extracted. The following table shows the values of n which were found. The mean number of particles in the tube and the trajectory of the particle flux n over time in these three cases can be seen on the next page in the Figures 20, 21 & 22.

Table 7: volume flux vs force

F / kJ mol^{-1} nm^{-1}	n / 1
50000	155
100000	253
250000	612

To get the volume flux Q_{sim} from the particle flux Φ_{flux} in the simulation, one has to divide by the medium number of water molecules per volume $D \approx 33$ 1/nm^3,

$$Q_{sim} = \frac{\Phi_{flux}}{D} \tag{35}$$

One can extract the slip length b by fitting the modified Hagen-Poiseulle equation 19 to the simulated volume flux Q_{sim}.
The flow enhancement factor EF can then be calculated as

$$\mathrm{EF} = \frac{Q_{slip}}{Q_{continuum}} \tag{36}$$

Using the simulation data in the smallest nanotube (see also the flux plots 202122) the flow enhancement factor EF can be calculated as a function of the pressure difference.

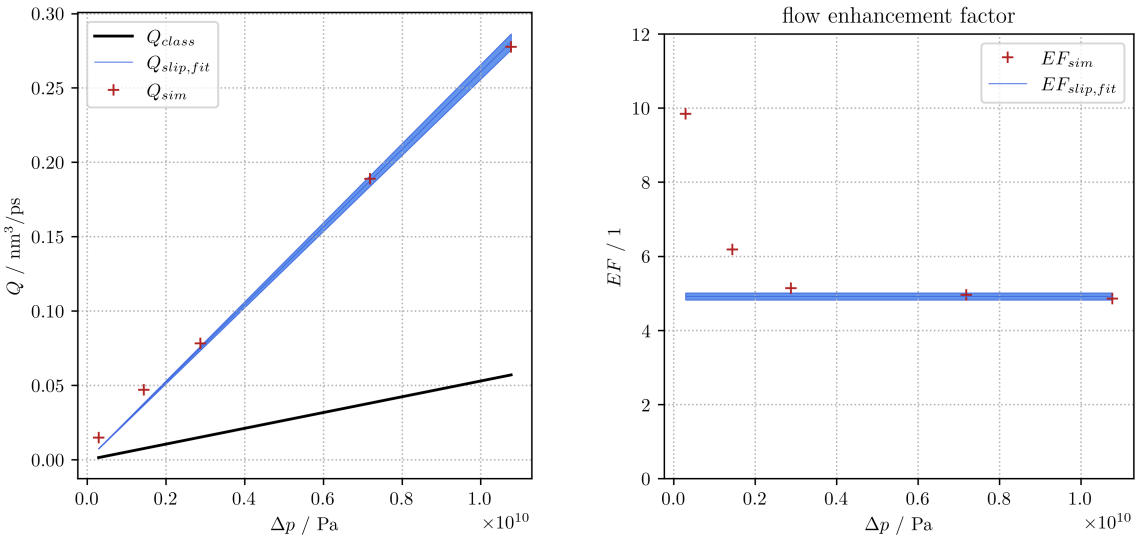

Figure 19: The classical, modified Hagen-Poiseuille and simulated volume flux in five simulations with different pull forces and the calculated flow enhancement factor.

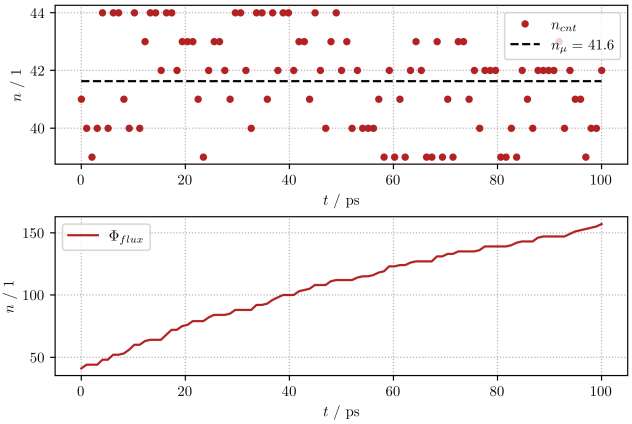

Figure 20: On top the current number n of water molecules in the nanotube is shown in a simulation with a pull force $F = 50000$ kJ/(mol nm). Below, the cumulative particle flux Φ_{flux} through the channel is shown.

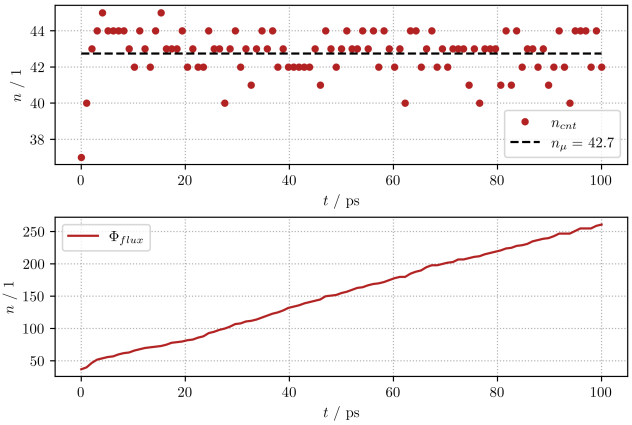

Figure 21: On top the current number n of water molecules in the nanotube is shown in a simulation with a pull force $F = 100000$ kJ/(mol nm). Below, the cumulative particle flux Φ_{flux} through the channel is shown.

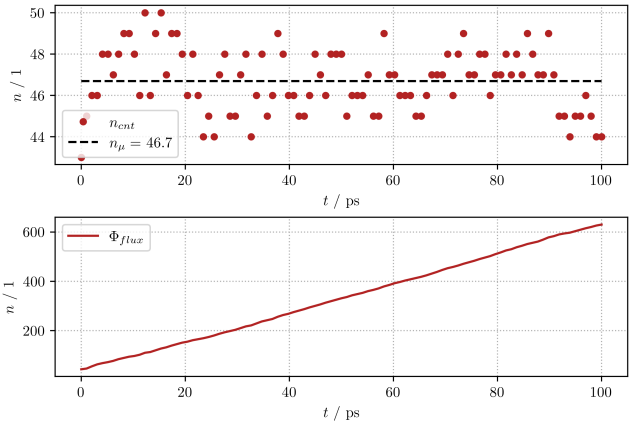

Figure 22: On top the current number n of water molecules in the nanotube is shown in a simulation with a pull force $F = 250000$ kJ/(mol nm). Below, the cumulative particle flux Φ_{flux} through the channel is shown.

5.3.1 Variation of the carbon bond spring constant

To study the effect of different C-C bond parameters and also to try and model more flexible channels, the harmonic spring constant k_b was varied (see chapter 5.1). These variations were carried out in the (13,0) system. Firstly, the dependence of the radius of the atoms of the nanotube were considered. In the following Figures 23 & 24 the positions of the carbons are displayed during two different simulations.

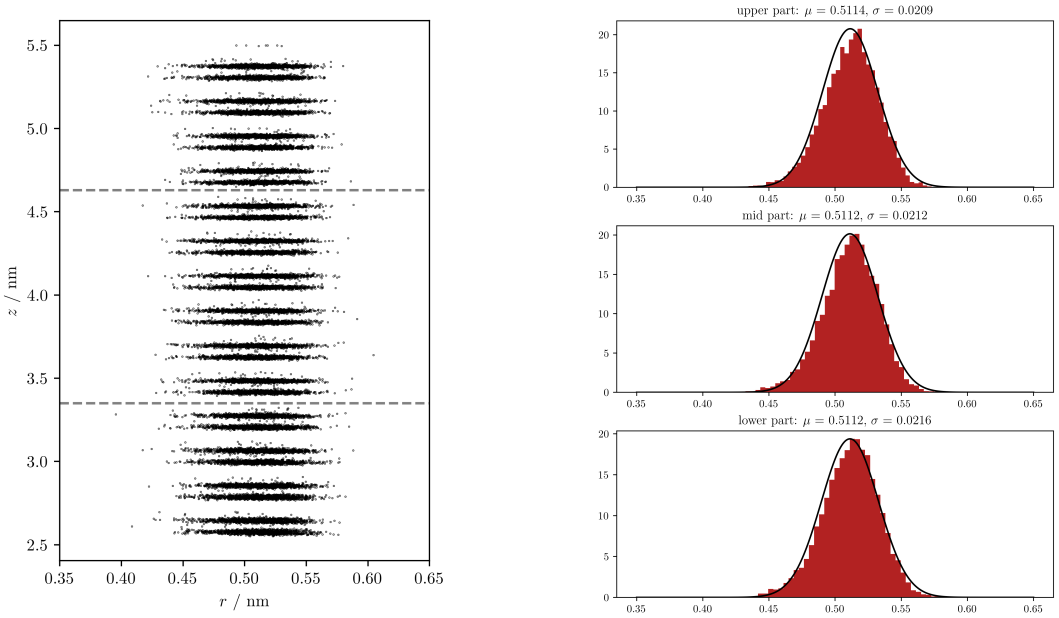

Figure 23: Position of the carbon atoms in a 100ps simulation at a realistic spring constant of $k_b = 3200000$ kJ mol^{-1}nm^{-2} and a pull force $F = 100000$ kJ mol^{-1}nm^{-1}.

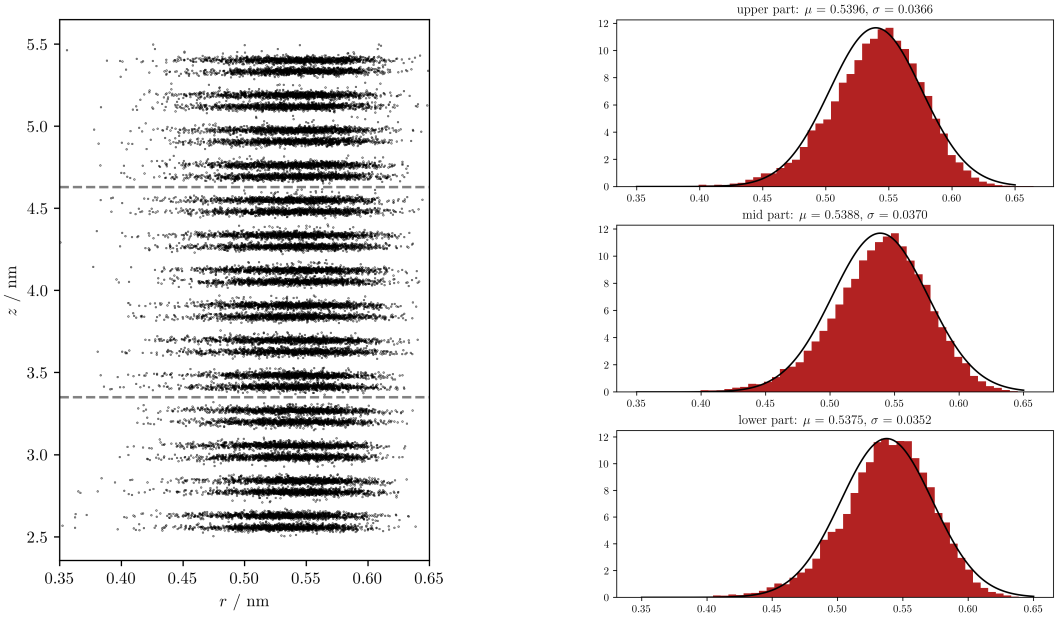

Figure 24: Position of the carbon atoms in a 100ps simulation at a very flexible spring constant of $k_b = 100000$ kJ mol^{-1}nm^{-2} and a pull force $F = 100000$ kJ mol^{-1}nm^{-1}.

The values of the mean carbon radius r_μ^C and the standard deviation σ_{r^C} of the fitted normal distribution to the histograms of the different nanotube parts were extracted. The range of magnitude of different spring constant k_b was simulated from very flexible constantly twisting to stiffer than realistic tubes. The results of these simulations are shown in the following Figure 25.

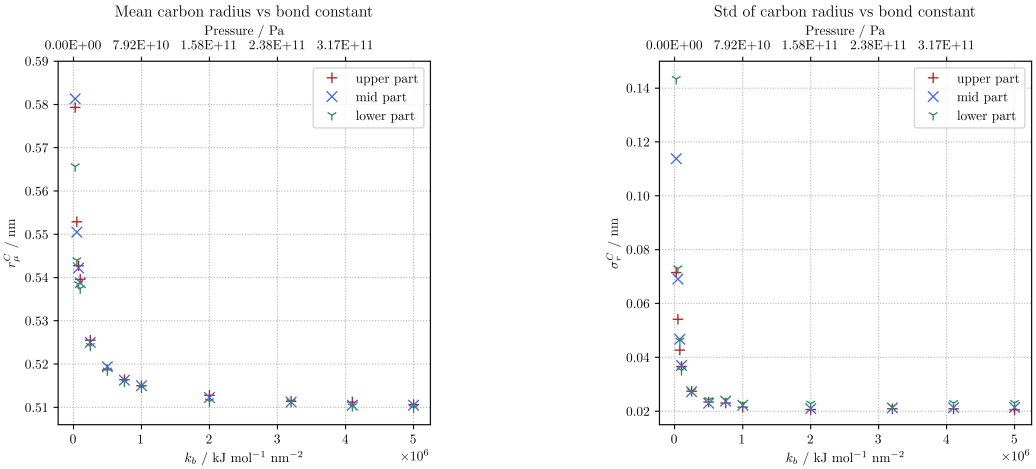

Figure 25: The mean carbon radius r_μ^C and the standard deviation σ_{r^C} in the (13,0) nanotube as a function of the C-C spring constant k_b.

The mean velocity $\langle u_z \rangle$ and the mean radial position r_μ^W of the water inside of the channel were also calculated for the same simulations. Here, one can see a sharp drop in the water velocity due to the increased flexing of the nanotube at low spring constants, which was observed in the animations of the system.

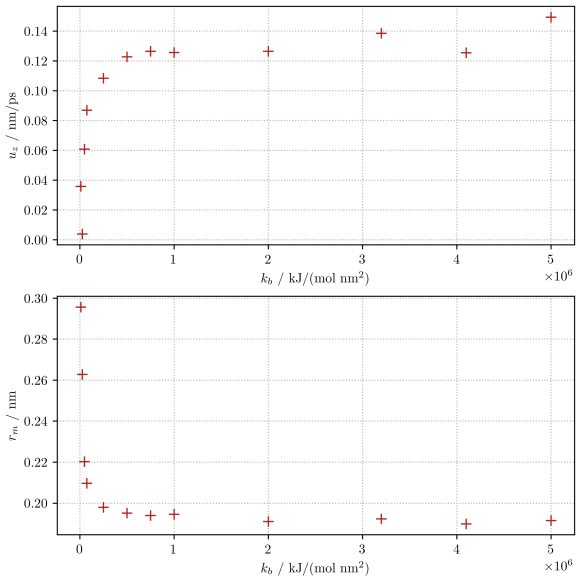

Figure 26: The mean axial velocity $\langle u_z \rangle$ and the mean radius r_μ^W of the water in the (13,0) nanotube as a function of the C-C spring constant k_b.

5.3.2 Water mean radial position with increased pressure

Out of the simulations, which were used to check the microscopic Hagen-Poiseuille law the mean radius r_μ^W of the waters inside the nanotube was also calculated. Since these simulation runs were carried out once with an NPT step and once without it, these two cases can also be compared.

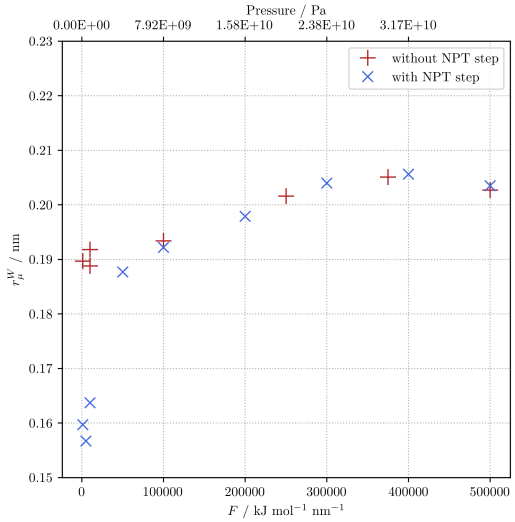

Figure 27: The mean water radius r_μ^W against the applied pull force F

5.4 Finite element method

A finite element model was created to quantify and visualise the flow fields inside nanotubes using the continuum Stokes equation.

5.4.1 Setup, parameters and boundary conditions

A simulation setup was created in which the finite element mesh (see, for example Figure 28), the in/out-flow boundary conditions, the velocity slip-condition as well as an space dependent viscosity can be varied as needed. Unfortunately, more complex simulations could not be carried out to limit the scope of this work. The finite element implementation was planned to be used to create a space dependent viscosity model to better describe flows inside nanotubes and to iterate over different boundary conditions. A model with added reservoirs was also added but shall not be shown in this work. To illustrate the capabilities of this finite element setup, the following case study will be shown.

parameter	value
d_{CNT}	2,35 nm
l_{CNT}	5 nm
η_{WAT}	1 mPa s
v_{slip}	0,05 nm/ps
v_{inflow}	0,09 nm/ps
$v_{outflow}$	0,09 nm/ps

Table 8: Simulation parameters

5.4.2 Simulation results

The simulation results using the finite element code FEnics (the code is in the Appendix) of the described model problem can be seen in the following Figure 28. Here, the absolute magnitude of the velocity field is plotted on each degree of freedom and linearly interpolated. One can see the development of a boundary layer on the in and outflow due to the prescribed constant inflow conditions.

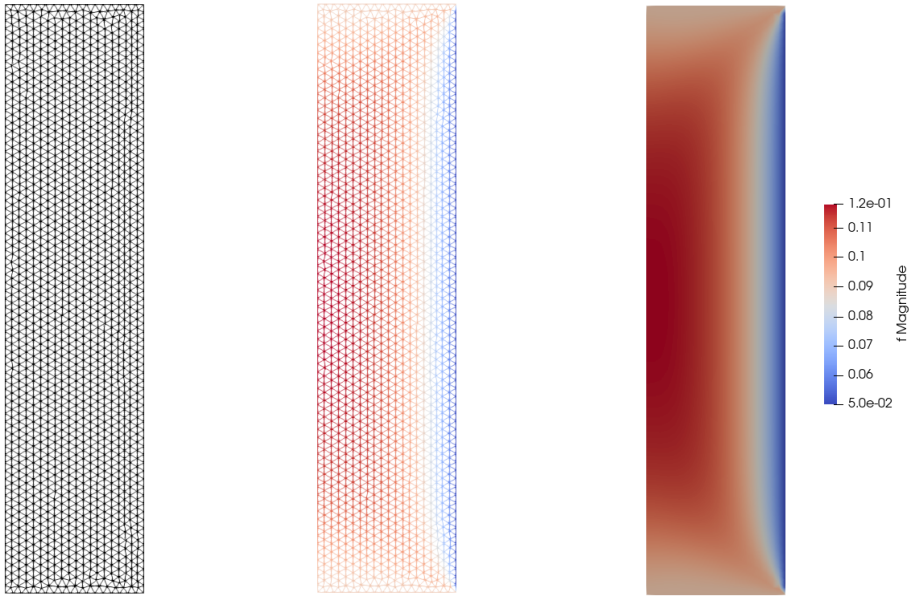

Figure 28: The used simulation mesh, the velocity solution superimposed on the mesh and the interpolated velocity field in the nanotube.

The axial velocity component u_z was then extracted on different radial slices through the domain. These slices and the corresponding velocity profile are shown in figure 29.

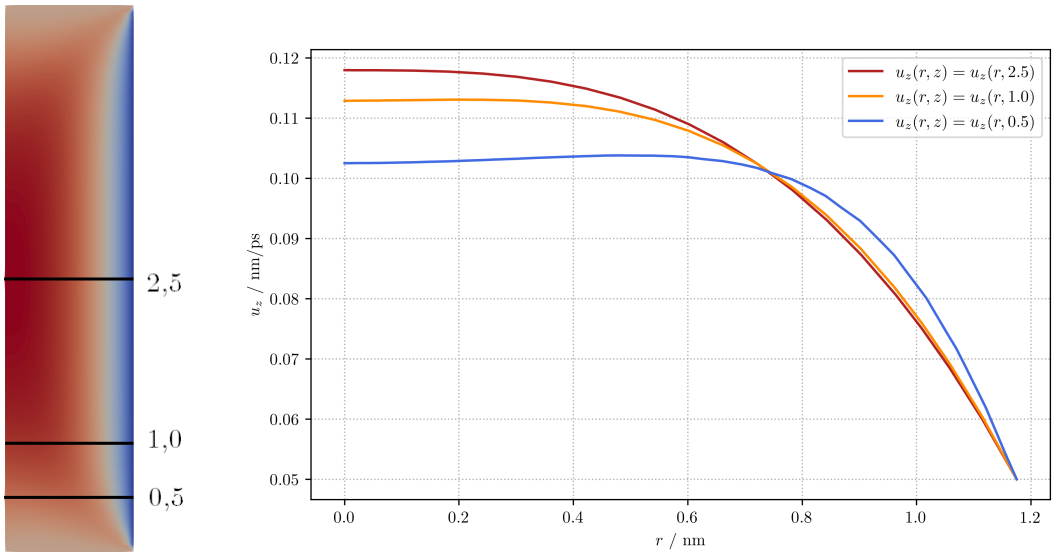

Figure 29: The velocity field solution with added slices through the domain, on the right the line plots of the velocity profiles along these slices.

6 Discussion

In this chapter, a comparison of results found in this work to the literature will be given. First, the application of continuum theory on the microscopic scale will be questioned. Then the large spread of observed slip lengths and corresponding enhanced flow rates in theoretical, experimental and computational studies shall be highlighted. At last, a quick overview on experimental studies is given to round off this work with a showcase of experimental methods used to measure microscopic flows through carbon nanotubes.

6.1 On the validity of continuum theory at nanometer scales

Due to new manufacturing capabilities on the microscale, a rise in studies on nanofluidic devices and the application of continuum mechanics to describe the relevant flows has emerged. Many authors try to give lower bounds for the applicability of the Navier-Stokes equations. The following three rules of thumb were taken directly out of the work [22]:

- *Above 10 nm confinement, fluid transport is governed by continuum hydrodynamic equations, with coupling to ion transport and surface effects.*
- *Below 10 nm –the domain of so-called single-digit nanopores – thermal fluctuations and electrostatic correlations are increasingly important, challenging continuum and mean-field theory.*
- *In few nanometre confinement, fluid structuring effects and correlations play an overwhelming role.*

In another study [12], the author finds that

- *The Navier-Stokes equations with stick boundary conditions apply in channels larger than 150 molecular diameters ($\simeq$50 nm) regardless of the strength of the fluid-wall binding energy.*

Since this work focused only on systems with a size of a few nanometers, big deviations from continuum theory with standard no-slip boundary conditions are expected. The importance of hydrogen bonding and van der Waals forces at the interplay of water molecules within nanotubes is apparent. The mentioned structuring effect was found to be essential to understand the velocity profiles inside the nanotube. As expected, it was also found that these structuring effects get less important as the size of the nanotube increases. In bigger nanotubes, the structuring effect is the most present in the regions near the wall and decreases radially. Continuum theory nevertheless gives a reference to which one can compare molecular dynamics simulation, although at these length scale continuum theory is also not meant to describe the phenomena of molecular processes. The Hagen-Poiseuille law especially showed itself to be a good benchmark to compare the pressure-flow characteristics of nanoflows.

6.2 Variations in observed slip lengths

To compare the relatively small slip lengths found in this work to literature values many factors have to be taken into account. The applied pressure, bond parameters, water models and tube flexibility have an effect on the calculated slip length. In other studies it

was also found that the chiral-indices (n,m) of the nanotubes have a considerable impact on the slip length. A main problem of the entire field is that it is difficult to have reproduceable simulation and experimental results. Over the years, many authors have run different setups with widely scattered results. The following Figure 30, which plots the observed slip length across a range of studies, shows just how big the variations really are. For some tube diameters the slip length varies three orders of magnitude.

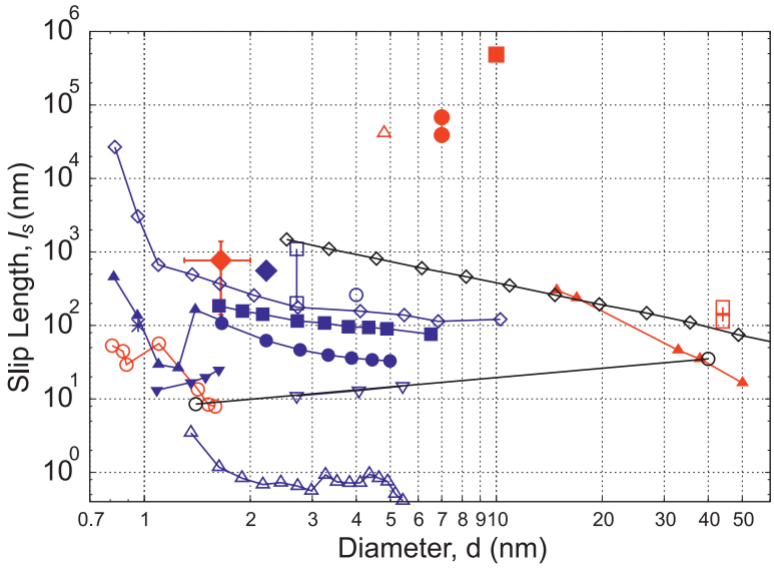

Figure 30: Slip length b from simulations (blue), theoretical predictions (black) and experiment (red). This image was reproduced from [3]

Comparing simulation results with experimental studies also does not seem to shed much light on which parameters offer the best description of reality. This is partly due to the fact that experimental results also scatter dramatically. In the next section, two experimental setups will be shown.
One potential problem in data analysis, which was also encountered during this thesis, is the method of fitting a parabola to the simulated velocity profiles. At low pressure gradient the resulting velocity profiles are very hard to fit because of the high noise inflicted by thermal fluctuations. This is also reported in the literature [3]. Even long simulation times in the order of tens of nanoseconds often result in small fluid velocity gradient at low speed. Fitting this kind of data can result in any slip length. These results are highly unpredictable. Since in this work very high pressures were used with smaller simulation times the statistics are worse than in other studies. Nevertheless, the high velocity gradients induced by such pressures resulted in small slip lengths. Due to these difficulties it seems unlikely that a consensus in observed slip lengths and flow enhancements of theory, experiment and simulation will be found anytime soon.

6.3 Experimental methods for nanoflows

Precise measurement of flow rates in nanocapillaries through direct flow rate measurement have been conducted but are very difficult because of the small flow rates in the range of $\approx$ 1 pl/s and the required probing sensitivity. The experimental study [23] uses an alternative measurement approach. They use an external liquid flow containing tracer particles to superimpose the jet flow through a carbon nanotube (see Figure 31). This kind of jet flow injected in a outside fluid medium is called a Landau–Squire jet. The velocity field of the outside flow was then measured using the injected tracer particles.

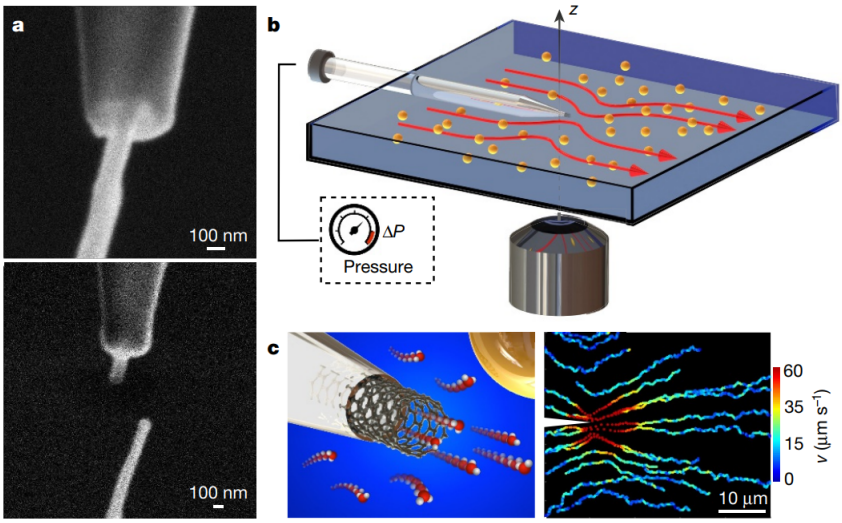

Figure 31: Experimental setup using a Landau–Squire jet. [23]

This study carried out a range of experiments by varying the carbon nanotube radius. The resulting measured flow enhancement factor $k_{NT}/k^{ref}_{no-slip}$ and the corresponding slip length b are shown in the following Figure 32.

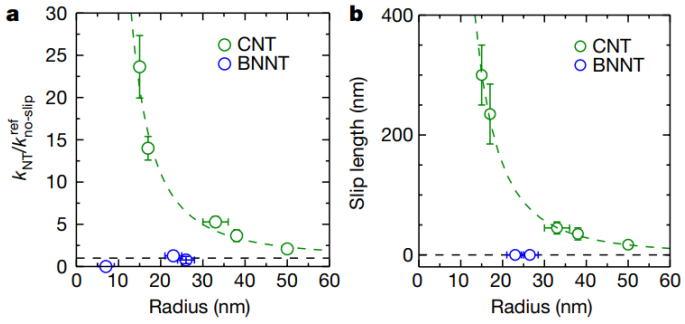

Figure 32: Slip length b [23]

Another study [24] which focuses on the ionic transport in carbon nanotubes used an experimental setup (see Figure 33) where a single nanotube was fixated between two reservoirs using photoresist. The protruding ends of the tube were then cut off using a focused ion beam.

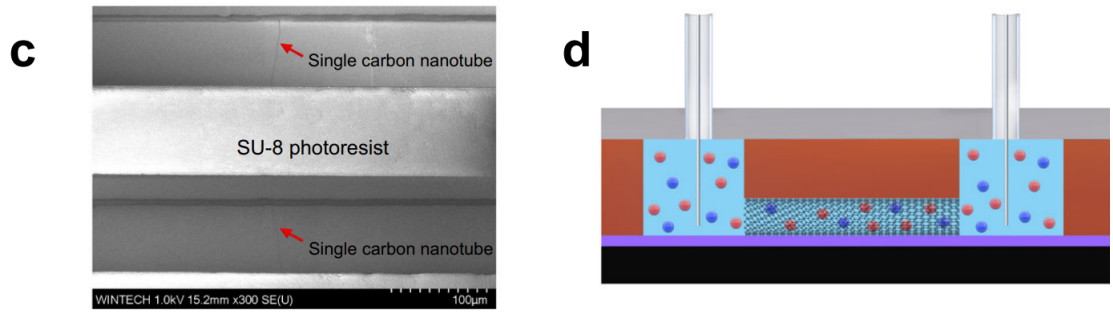

Figure 33: Experimental setup using a nanotube casted in photoresist. [24]

The slip length b of this system was then extracted out of the measured charge density. Figure 34 shows the results gained by this work and other experimental studies in the microscopic regime.

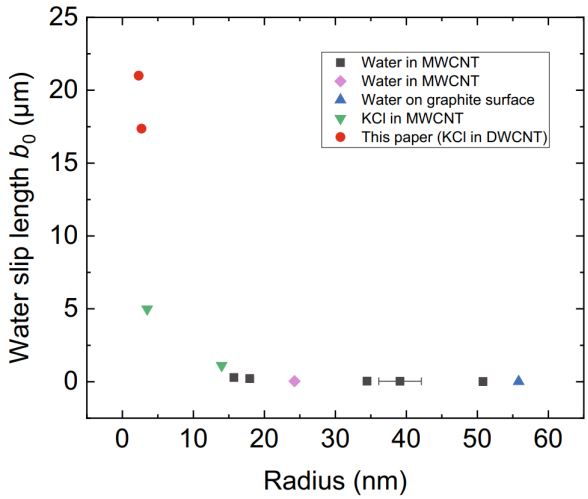

Figure 34: Slip length b [24]

As already stated in section 6.2, results for the flow enhancement factor and the slip length scatter dramatically between experiments and simulations. This is well-known in the field and is a frequent topic of discussion.

7 Conclusion

The obtained values for the slip length and the resulting flow enhancements appear smaller than in previous simulations. It is unclear what differences in simulation settings cause this discrepancy. The linear nature of the Hagen-Poiseuille law and its slip flow equivalent were shown to hold up to very high pressures and also work in very small nanotubes. The variation of the harmonic bond constant showed effects on the velocity and on the mean radii of water molecules and the nanotube. Against expectations a increase in flexibility caused a decrease in observed volume flux. This is thought to be caused by increased water-wall interactions. Despite the significant progress made in understanding the interactions of water in carbon nanotubes, several challenges and unanswered questions remain. Further research is needed to understand the role of water models and their interaction with carbon. The large spread of observed slip lengths in simulations with different simulation settings makes it difficult to gain knowledge about individual system characteristics. The method of calculating slip lengths by fitting parabolic profiles seems very inconsistent at small pressures and should be questioned. Due to these facts the field does not agree on the amount of flow enhancement which exists in carbon nanotubes. At least the existence of some form of slip and corresponding enhancements is broadly accepted. It is safe to say that the study of microscopic confined water flows will continue to gain important insights to biological systems. As nanofluidics is a relatively new field, research in innovative technical devices which harness microscopic effects will increase in the next decades. Only the future can tell what impact on humanity this research field will have. Most importantly are, of course, more experimental studies with capabilities of probing water transport at the nanoscale to validate the theoretical and computational results presented in the literature. Only such controlled experiments can shine a light on the true nature of nanoflows and select correct theoretical models.

8 Bibliography

References

[1] Franz Durst. *Fluid Mechanics - An Introduction to the Theory of Fluid Flows*. Wiesbaden: Springer Berlin Heidelberg, 2022. ISBN: 978-3-662-63913-9.

[2] Lyderic Bocquet and Elisabeth Charlaix. "Nanofluidics, from bulk to interfaces". In: *Chemical Society reviews* 39 (Mar. 2010), pp. 1073–95. DOI: 10.1039/b909366b.

[3] Sridhar Kannam. "Modeling slip and flow enhancement of water in carbon nanotubes". In: *MRS Bulletin* 42 (Apr. 2017), p. 283. DOI: 10.1557/mrs.2017.61.

[4] Douwe Jan Bonthuis et al. "Theory and simulations of water flow through carbon nanotubes: prospects and pitfalls". In: *Journal of Physics: Condensed Matter* 23.18 (Apr. 2011), p. 184110. DOI: 10.1088/0953-8984/23/18/184110. URL: https://dx.doi.org/10.1088/0953-8984/23/18/184110.

[5] Tim Myers. "Why are slip lengths so large in carbon nanotubes?" In: *Microfluidics and Nanofluidics* 10 (May 2011), pp. 1141–1145. DOI: 10.1007/s10404-010-0752-7.

[6] Simon Gravelle et al. "Optimizing water permeability through the hourglass shape of aquaporins". In: *Proceedings of the National Academy of Sciences* 110.41 (2013), pp. 16367–16372. DOI: 10.1073/pnas.1306447110.

[7] Charlotte I. Lynch, Shanlin Rao, and Mark S. P. Sansom. "Water in Nanopores and Biological Channels: A Molecular Simulation Perspective". In: *Chemical Reviews* 120.18 (2020). PMID: 32841020, pp. 10298–10335. DOI: 10.1021/acs.chemrev.9b00830. eprint: https://doi.org/10.1021/acs.chemrev.9b00830. URL: https://doi.org/10.1021/acs.chemrev.9b00830.

[8] J. Clerk Maxwell. "On Stresses in Rarefied Gases Arising from Inequalities of Temperature. [Abstract]". In: *Proceedings of the Royal Society of London* 27 (1878), pp. 304–308. ISSN: 03701662. URL: http://www.jstor.org/stable/113680 (visited on 05/21/2023).

[9] David Morris, Lawrence Hannon, and Alejandro Garcia. "Slip length in a dilute gas". In: *Physical review. A* 46 (Nov. 1992), pp. 5279–5281. DOI: 10.1103/PhysRevA.46.5279.

[10] Jana Wedel et al. "A specific slip length model for the Maxwell slip boundary conditions in the navier–stokes solution of flow around a microparticle in the no-slip and slip flow regimes". In: *Theoretical and Computational Fluid Dynamics* 36.5 (2022), pp. 723–740. DOI: 10.1007/s00162-022-00627-w.

[11] Nikita Kavokine, Roland Netz, and Lyderic Bocquet. "Fluids at the Nanoscale: from continuum to sub-continuum transport". In: (Nov. 2020).

[12] Chong Liu and Zhigang Li. "On the validity of the Navier-Stokes equations for nanoscale liquid flows: The role of channel size". In: *AIP Advances* 1.3 (July 2011). 032108. ISSN: 2158-3226. DOI: 10.1063/1.3621858. eprint: https://pubs.aip.org/aip/adv/article-pdf/doi/10.1063/1.3621858/12995233/032108_1_online.pdf. URL: https://doi.org/10.1063/1.3621858.

[13] Aris Chatzichristos and Jamal Hassan. "Current Understanding of Water Properties inside Carbon Nanotubes". In: *Nanomaterials* 12.1 (2022). ISSN: 2079-4991. DOI: 10.3390/nano12010174. URL: https://www.mdpi.com/2079-4991/12/1/174.

[14] Mark James Abraham et al. "GROMACS: High performance molecular simulations through multi-level parallelism from laptops to supercomputers". In: *SoftwareX* 1-2 (2015), pp. 19–25. ISSN: 2352-7110. DOI: https://doi.org/10.1016/j.softx.2015.06.001. URL: https://www.sciencedirect.com/science/article/pii/S2352711015000059.

[15] H. J. C. Berendsen, J. R. Grigera, and T. P. Straatsma. "The missing term in effective pair potentials". In: *The Journal of Physical Chemistry* 91.24 (1987), pp. 6269–6271. DOI: 10.1021/j100308a038. eprint: https://doi.org/10.1021/j100308a038. URL: https://doi.org/10.1021/j100308a038.

[16] Pekka Mark and Lennart Nilsson. "Structure and Dynamics of the TIP3P, SPC, and SPC/E Water Models at 298 K". In: *The Journal of Physical Chemistry A* 105.43 (2001), pp. 9954–9960. DOI: 10.1021/jp003020w. eprint: https://doi.org/10.1021/jp003020w. URL: https://doi.org/10.1021/jp003020w.

[17] H. J. C. Berendsen et al. "Molecular dynamics with coupling to an external bath". English. In: *Journal of Chemical Physics* 81.8 (1984), pp. 3684–3690. ISSN: 0021-9606. DOI: 10.1063/1.448118.

[18] J. Hake M. S. Alnaes J. Blechta and A. Johansson. "The FEniCS Project Version 1.5". In: *Archive of Numerical Software* 3 (2015). DOI: 10.11588/ans.2015.100.20553.

[19] Susanne Brenner and Ridgway Scott. *The Mathematical Theory of Finite Element Methods* -. Berlin Heidelberg: Springer Science Business Media, 2007. ISBN: 978-0-387-75933-3.

[20] Mats G. Larson and Fredrik Bengzon. *The Finite Element Method: Theory, Implementation, and Applications* -. Berlin Heidelberg: Springer Science Business Media, 2013. ISBN: 978-3-642-33287-6.

[21] José Urquiza, André Garon, and Marie-Isabelle Farinas. "Weak imposition of the slip boundary condition on curved boundaries for Stokes flow". In: *Journal of Computational Physics* 256 (Jan. 2014), pp. 748–767. DOI: 10.1016/j.jcp.2013.08.045.

[22] Nikita Kavokine, Roland R. Netz, and Lydéric Bocquet. "Fluids at the Nanoscale: From Continuum to Subcontinuum Transport". In: *Annual Review of Fluid Mechanics* 53.1 (2021), pp. 377–410. DOI: 10.1146/annurev-fluid-071320-095958. eprint: https://doi.org/10.1146/annurev-fluid-071320-095958. URL: https://doi.org/10.1146/annurev-fluid-071320-095958.

[23] Eleonora Secchi et al. "Massive radius-dependent flow slippage in carbon nanotubes". In: *Nature* 537.7619 (2016), pp. 210–213. DOI: 10.1038/nature19315.

[24] Guandong Cui et al. "Enhanced osmotic transport in individual double-walled carbon nanotube". In: *Nature Communications* 14.1 (2023). DOI: 10.1038/s41467-023-37970-3.

[25] James Ahrens, Berk Geveci, and Charles Law. "ParaView: An End-User Tool for Large Data Visualization". In: *Visualization Handbook*. ISBN 978-0123875822. Elesvier, 2005.

9 Appendix

Due to large amount of code written in the molecular dynamics and finite element parts of this thesis, it is not practical to attach it in the appendix. Here I give a short description of each created code file. The code can be found on the following repository: `https://github.com/brunner-th/WaterFlowsInCarbonNanotubes`.

9.1 MD-Code

- **gro_file_create.py**

Creation of the .gro- and .itp-files which contain all information about the geometry, bonds and potentials.

- **edr_reader.py**

Reading in .edr-files which contain simulated values of the potential energy, pressure and temperature. For this the library panedr (`https://github.com/MDAnalysis/panedr`) was used.
Creation of the all the plots given in this thesis was done in the following files:

- **carbon_radius.py**
- **cnt_plots.py**
- **flow_enhancement_factor.py**
- **slip_length_vs_force.py**
- **cnt_heatmap_with_stepwise_mean.py**
- **small_cnt_plot_speed_vs_bondk.py**
- **cnt_plot_speed_vs_pressure_from_pull_force.py**
- **cnt_volume_flux_vs_time.py**

9.2 FE-Code

A few test programs were written to learn the FEnics framework and get the simulations to run. These shall not be included in the repository. A good introduction to FEnics can be found on the projects documentation page.

- **stokes_cnt_axisymm_var_viscosity.py**

To read the created .xdmf-files the open-source software ParaView [25] was used.